iScience

CellPress
OPEN ACCESS

Article

Intelligent soft robotic fingers with multi-modality perception ability

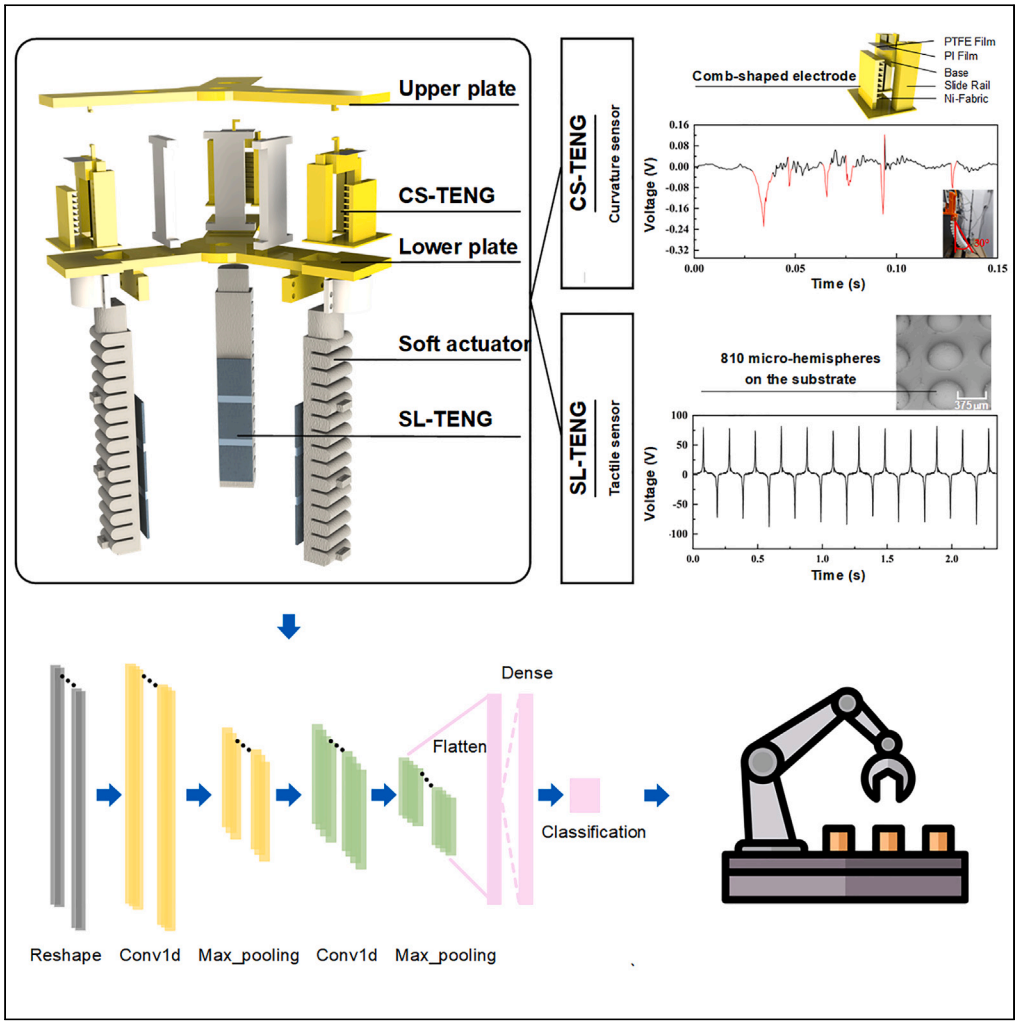

Tongjing Wu, Haitao Deng, Zhongda Sun, Xinran Zhang, Chengkuo Lee, Xiaosheng Zhang

elelc@nus.edu.sg (C.L.)
zhangxs@uestc.edu.cn (X.Z.)

Highlights

Three structures of SL-TENG and CS-TENG are developed to serve as sensors

The developed sensors successfully achieve multifunctional passive sensing capabilities

Soft manipulator with developed sensors achieves object recognition with 98.6% accuracy

Wu et al., iScience 26, 107249
August 18, 2023
https://doi.org/10.1016/j.isci.2023.107249

iScience

CellPress
OPEN ACCESS

Article

Intelligent soft robotic fingers with multi-modality perception ability

Tongjing Wu,[1,2] Haitao Deng,[1] Zhongda Sun,[2] Xinran Zhang,[1] Chengkuo Lee,[2,*] and Xiaosheng Zhang[1,3,*]

SUMMARY

In the context of industry 4.0, automatic sorting is becoming prevalent in production lines. Herein, we developed a bionic sensing system to achieve real-time object recognition. The system consists of 9 single-layer triboelectric nanogenerators (SL-TENGs) as touch sensors and 3 comb-shaped TENGs (CS-TENGs) as bending sensors, with a sensitivity of 110 V/kPa and stable output after 20,000 press cycles. These sensors were attached to a manipulator composed of three soft actuators, serving as soft robotic fingers. An enhanced electrical output of these sensors was achieved successfully, demonstrating their feasibility in detecting grasping location, contact pressure, and bending curvature. A one-dimensional convolutional neural network (1D-CNN) with 98.96% accuracy extracted information from the sensors, enabling the manipulator to serve as an intelligent sensing system with multi-modality perception ability. This robotic manipulator successfully integrated TENG-based self-powered sensors, soft actuators, and artificial intelligence, demonstrating the potential for future digital twin applications, particularly in automatic component sorting.

INTRODUCTION

With the development of 5G technology, the cost of large-scale data transmission has dropped sharply; thus smart houses and smart manufacturing based on the internet of things (IoT) framework where a large number of sensors are used for real-time signal transmission and analysis have been developed rapidly.[1–5] Based on artificial intelligence (AI) and IoT, the concept of digital twin is proposed, which is of great significance in the field of intelligent manufacturing.[6–9] A major application of digital twin is components sorting in unmanned factories, where robotic manipulators are widely used. In the past few years, soft robotics has become an emerging research topic, providing new possibilities for addressing these tasks.[10–14] Compared with conventional rigid robotics, soft robots offer enhanced elasticity, adaptability, and reinforcement in accomplishing tasks.[15–17]

Traditional components sorting is based on visual sensors, which has many shortcomings. For example, the extracted information dimension is limited, and it is unable to make accurate recognition when two objects are similar in appearance. Besides, in a dim environment, the recognition performance of the visual sensors is greatly reduced.[18] Thus, finding another type of sensor to compensate for the shortcomings of visual sensors has become an urgent issue in this field. Since the manipulator is composed of soft actuators for high compliance and dexterity, the high nonlinear deformation and no-joint structure make it difficult to use traditional sensors, like encoder, potentiometer, etc. Till now, the feasible solutions are sensors based on piezoelectricity,[19–24] electromagnetic effect[25–28] and conductive nanocomposites,[29] optical fiber,[30] and triboelectricity.[31] However, different kinds of mechanisms have unique working conditions and output properties. For example, Hall sensor is necessary when using electromagnetic effect, which makes the fabrication of soft robot and the signal processing more complex. Among them, the self-powered sensor based on TENG is a good choice, which has many advantages over other kinds of sensors, like high output amplitude and wide material choices.[32–38] In fact, TENG-based sensors have been widely used in wearable devices.[39–48] In the field of soft robots, they are attracting more and more attention and many structures have been proposed in recent years.[49–51] By integrating a TENG on different parts of the soft robot, e.g., front,[52] bottom,[53] or even the chamber,[13] electrical outputs can be generated from a single stimulus input, thus realizing the function of detecting obstacle,[52] location,[54,55] curvature,[49] or even humidity.[56]

[1]School of Integrated Circuit Science and Engineering, University of Electronic Science and Technology of China, Chengdu 611731, China

[2]Department of Electrical and Computer Engineering, National University of Singapore, 4 Engineering Drive 3, Singapore 117576, Singapore

[3]Lead contact

*Correspondence: elelc@nus.edu.sg (C.L.), zhangxs@uestc.edu.cn (X.Z.)

https://doi.org/10.1016/j.isci.2023.107249

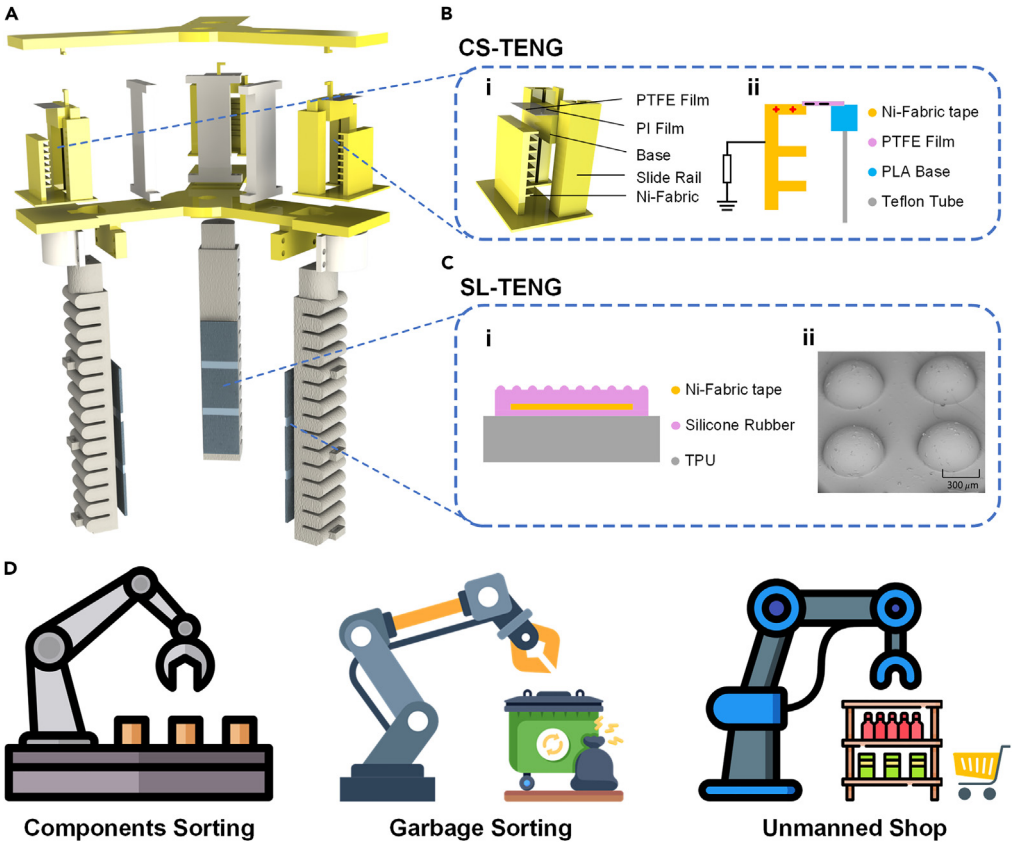

Figure 1. Physical characteristics of the developed sensing system

(A) Explosion view of the manipulator, consisting of three CS-TENGs, nine SL-TENGs, and three soft actuators.

(B) The as-fabricated CS-TENG sensor and the basic structure. (i) The model of CS-TENG. (ii) The sketch of CS-TENG.

(C) The as-fabricated SL-TENG sensor and the basic structure. (i) The sketch of SL-TENG. (ii) The SEM image of the silicone rubber.

(D) Schematic diagram of potential applications that can be enabled by the developed sensing system.

In this work, we propose a robotic manipulator with three soft actuators. Owing to the high flexibility of thermoplastic polyurethane (TPU) and the hollow structure, the manipulator can grasp various kinds of objects easily and the force can be adjusted by the air pressure precisely. In addition, we develop two kinds of TENG-based sensors (named single-layer TENG [SL-TENG] and comb-shaped TENG [CS-TENG]), which can serve as the tactile sensor and bending sensor, respectively. For SL-TENG, we propose two structures, i.e., pyramid microstructure and hemispherical microstructure. Due to the different electronegativity of components, contact pressure, and area, the outputs of the sensor will be different. For CS-TENG, we propose a slide rail structure with the comb-shaped electrode, which is working in a contact-separation mode. With this structure, by counting the number of peaks in the output signal, the curvature of the actuator can be deduced. The tri-actuator soft gripper is then integrated with TENG sensors. Finally, by leveraging the convolutional neural network for data analysis, the gripper is successfully demonstrated to realize object identification.

RESULTS AND DISCUSSION

Characterization of the developed sensing system

Figure 1A illustrates an exploded view of the manipulator, which consists of SL-TENG, CS-TENG, soft actuators, etc. There are three slide rails fixed on the lower plate, where an integrated electrode and polyimide (PI) film form the CS-TENG. Figure 1B shows the structure and working mechanism of CS-TENG. Once the polytetrafluoroethylene (PTFE) film rubs with the electrode, there will be a peak in the output, which realizes the function of curvature detecting. The structure of SL-TENG is shown in Figure 1C. There are

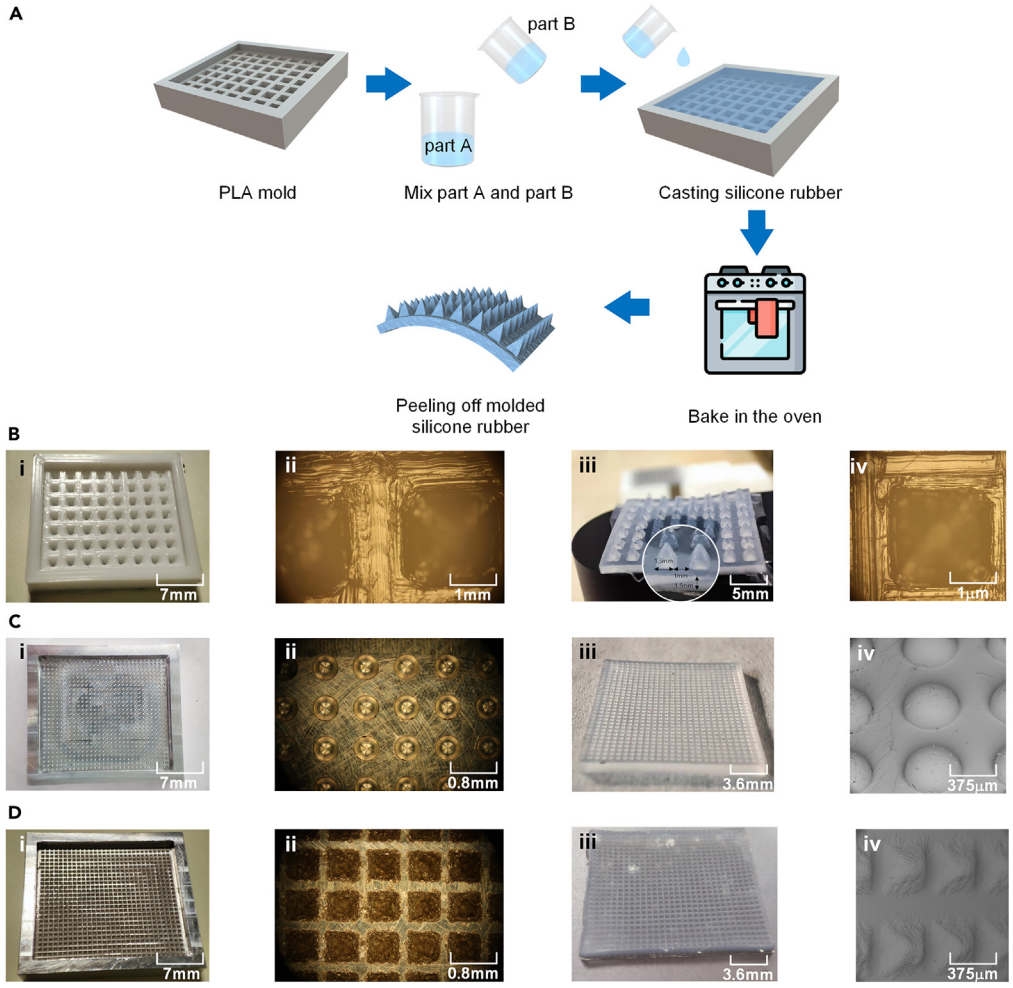

Figure 2. Fabrication of the SL-TENG

(A) Schematic illustration of the fabrication process flow chart of the developed SL-TENG with Pyramid Microstructure in a big size.

(B) Images of SL-TENG with Pyramid Microstructure in a big size. (i) Photograph of the mold. (ii) Optical microscope image of the mold. (iii) Photograph of the silicone rubber with Pyramid Microstructure in a big size. (iv) SEM image.

(C) Images of SL-TENG with Hemispherical Microstructure. (i) Photograph of the mold. (ii) Optical microscope image of the mold. (iii) Photograph of the silicone rubber with Hemispherical Microstructure. (iv) SEM image.

(D) Images of SL-TENG with Pyramid Microstructure in a small size. (i) Photograph of the mold. (ii) Optical microscope image of the mold. (iii) Photograph of the silicone rubber with Pyramid Microstructure in a small size. (iv) SEM image.

three SL-TENGs on each soft actuator, which can detect contact position, area, etc. Therefore, both the motion caused by self-actuation and external stimuli can be sensed. The proposed system can realize the function of digital twins. Hence, relevant applications related to digital twins can be realized, like components sorting, garbage sorting, unmanned shop, etc.

Fabrication of the SL-TENG

Pyramid microstructure in a big size

Figure 2A schematically illustrates the fabrication process flow of the SL-TENG with the pyramid microstructure in a big size. The bottom side length of each pyramid is 1.5 mm, and the height is 2.5 mm. The interval distance of each pyramid is 1 mm. To make this structure of tribo-skin, a polylactic acid (PLA) mold modeled in SolidWorks and printed by a 3D printer was needed first. In the next step, Eco-flex 00–30 silicone solutions were used (part A and part B were mixed at a ratio of 1:1 first) and poured into

the mold. After being evacuated to eliminate bubbles by a vacuum pump, the mold was put in the oven with the temperature at 40°C for 60 min. Finally, the molded silicone rubber was peeled off from the mold and stuck with the Ni-fabric tape. The TENG's length, width, and thickness are 25 mm, 22 mm, and 1.5 mm respectively. The images of the mold and sample are shown in Figure 2B.

Hemispherical microstructure

In this structure, the microstructure is changed into hemisphere. The radius is 250 μm, and the interval distance of each hemisphere is 300 μm. Since the minimum size in this structure reaches 250 μm, which has been far below the resolution of the 3D printer, computer numerical control (CNC) technique was used and the material of the mold was changed into aluminum this time. The pictures of the mold and the silicone rubber are shown in Figure 2C. The following step was the same as the counterparts in pyramid microstructure. The only difference is that since the mold is made of aluminum rather than PLA, the temperature of oven can be set to 70°C this time. And the waiting time was reduced to 15 min, which improved the efficiency of making SL-TENG.

Pyramid microstructure in a small size

In this structure, the bottom side length of each pyramid, the height, and the interval distance are reduced to 500 μm, 250 μm, and 300 μm, respectively. Therefore, CNC technique was necessary too. The steps are the same as those of hemispherical microstructure. The pictures of the mold and the silicone rubber are shown in Figure 2D.

Fabrication of the soft gripper

The soft gripper with a bellows-structured actuator was designed by software (Solidworks 2021). To ensure elastic property and output force, TPU filament with a hardness of shore 85 A was used to fabricate the soft actuator. The filament was extruded by Titan Extruder, and the printing temperature is 240°C with a corresponding low printing speed of 20 mm/s. The layer thickness was changed to 0.1 mm to guarantee the printing precision.

Configuration and working mechanism of the SL-TENG and CS-TENG sensors

Working mechanism and characterization of SL-TENG

Figure 3A schematically illustrates the working mechanism of SL-TENG, which is based on the triboelectrification and electrostatic induction effect. Since the soft manipulator keeps moving when working, TENG working in single-electrode mode is more suitable for the tactile sensor. As is shown in Figure 3A, SL-TENG is composed of silicone rubber and Ni-fabric tape. When an object comes in contact with the silicone rubber, electrons shift from the object's surface to rubber's surface due to the difference in electronegativity. As the object is leaving away, the two oppositely charged surfaces become separated and create a potential difference. The unscreened negative charges on the rubber surface drive free electrons flowing from the Ni-fabric tape to the ground and induce the accumulation of positive charges in the electrode, thus generating a current and voltage output. When the object is far away, an electrostatic equilibrium is attained and electrons stop moving. As the object approaches again, the separated distance between the silicone rubber and the object as well as their potential difference decrease. This process leads to a reverse electron flow from the ground to the embedded electrode and generates a voltage in the opposite direction.

Based on this basic structure, to increase the sensitivity of SL-TENG, we propose three new structures—pyramid microstructure in two sizes and hemispherical microstructure, which has been shown in the fabrication of the SL-TENG part. For pyramid microstructure in big size, there are 56 micro pyramids on the substrate. When the object contacts with the tribo-skin under different external forces, the variance of the contact area is much larger with the pyramid microstructure than that without microstructure. For pyramid microstructure in small size and hemispherical microstructure, thanks to the CNC technique, there are 810 microstructures on the substrate in total, which means that there will be a larger contact area when the object just contacts with the tribo-skin than the last structure, and thus the output amplitude will be increased dramatically. At the same time, the variance of the contact area is still large when the object touches the tribo-skin with different forces.

In order to investigate the performance of SL-TENG with the three structures and find which one is better, relevant tests had been taken. Figures 3B and Figure 3C show the test results. A vibration exciter, powered

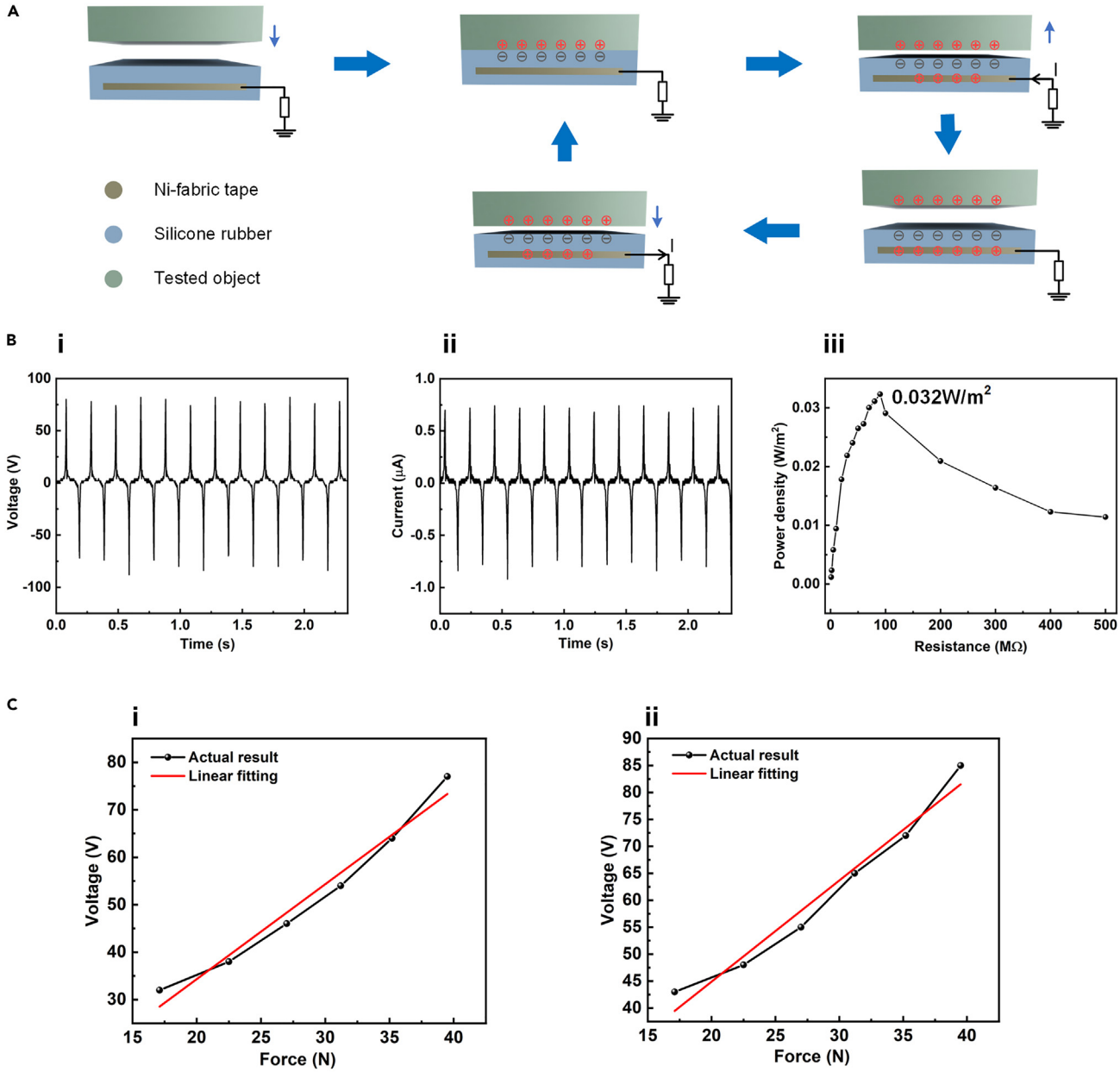

Figure 3. Working mechanism and characterization of SL-TENG

(A) The structure and working mechanism of SL-TENG.

(B) The electrical characteristic curves of SL-TENG with Hemispherical Microstructure. (i) Output voltage. (ii) Output current. (iii) The output power density on the loading resistors at various values from 1–500 MΩ connected to the triboelectric nanogenerator in parallel.

(C) Sensitivity to the pressure. (i) Hemispherical Structure. (ii) Pyramid Microstructure in a small size.

by a function generator, was used. A sine wave was set to be the excitation. The electrical characteristic curves of SL-TENG with the hemispherical microstructure are shown in Figure 3B. Those of other structures are shown in Figure S1. During the test, the frequency of the excitation was set to 2 Hz and the amplitude was set to 1 Voltage peak-peak (Vpp). According to the test results, the outputs of TENGs with smaller microstructures are much larger. Then, to test the sensitivity of the SL-TENG with the pyramid microstructure in small size and hemispherical microstructure, the whole TENG was covered by the platform at the end of the ejector pin so that the contact area was the same in every contact. The frequency was set to 2 Hz, and the amplitude was changed to represent different magnitudes of force. Then a force gauge was used to test

the corresponding force. Owing to the linear fitting done on the data point in Figure 3C, the hemispherical structure is more sensitive to pressure than the pyramid microstructure in small size, though the output of the latter one is larger. Since the area of SL-TENG is 0.055 m^2, the sensitivity of SL-TENG with the hemispherical microstructure is 110 V/kPa while the sensitivity of SL-TENG with the pyramid microstructure in small size is 103 V/kPa. Therefore, compared with pyramid microstructure in small size, the sensitivity of SL-TENG with the hemispherical microstructure has increased by 7%. This is because the contact area variation is larger for hemispherical structure, which is consistent with the experimental results of other groups.[57] The comparison of each structure has been listed in Table S1. Since high sensitivity is more important than high output for object recognition, SL-TENG with hemispherical microstructure is used in the soft robot. The other properties of SL-TENG were also tested, including thermal stability and humidity stability. The results are shown in Figure S2, which shows that SL-TENG can work normally in high-temperature and high-humidity environment. The robustness of SL-TENG with the hemispherical microstructure was also tested. The force gauge was used to press SL-TENG 20,000 times. The outputs of SL-TENG during the first few presses and after 20,000 presses are shown in Figure S2. The outputs are almost the same, which demonstrates good robustness of SL-TENG. Besides, the comparison of the proposed SL-TENG against other solutions has been listed in Table S2.

Working mechanism and characterization of CS-TENG

Inspired by the moving mode of the soft manipulator, a sliding TENG with combed electrodes in single-electrode mode is proposed. Figure 4A shows the basic structure and the working mechanism. The Teflon tube is connected with the end of the soft manipulator. When the manipulator bends, the Teflon tube will be pulled down, and thus the PLA base, which is fixed in a slide rail, will go down too. A kind of tribo-material is fixed on the PLA base, which will rub with the combed electrode during the process of bending. Due to the triboelectric effect, once the tribo-material rubs with the electrode, there will be a peak in the output. By counting the number of peaks, the number of electrodes that rub with the tribo-skin can be found. Since the distance between the electrodes is known, the moving distance of the base can be calculated, which is equal to the moving distance of the end of soft manipulator. In this way, the curvature of soft manipulator can be deduced. Since it is very difficult to guarantee the same output of TENG when the bending degree is unchanged due to environmental interferences, the design will be complex if a strain sensor is used, by which the curvature is calculated by the amplitude. Nevertheless, by using the comb-structural TENG sensor, there must be peaks in the output regardless of the amplitude. Therefore, by counting the number of peaks, the curvature can be stably calculated. Several structures have been designed based on the basic one, which are shown in Figure S3. Among them, the best model is the fifth one.

The tribo-material is PTFE film, which has a very high electronegativity. A PI film is attached to the top of the base. To guarantee the friction and smoothness, 75 μm PI film is chosen and then covered with PTFE film. At the bottom of the base, there is a circular hole to fix the Teflon tube. On the top of the base, there is a hook to be connected with a spring. The other end of the spring is connected with the top component. There is also a slide rail to fix the moving direction of the base. Finally, to make the electrode more stable, which is conducive to reducing the clutter, the comb-shaped model is integrated with the slide rail. Ni-fabric tape is stuck on the protruding part of the printed model to serve as the electrode.

In the initial test, the Teflon tube was pulled down and the tribo-material rubbed with six electrodes. Only in the fifth model, all six peaks can be clearly found and there is almost no clutter, which is shown in Figure S4. Importantly, the waveform was very stable in this model. Regardless of the speed of pulling down, the clear peaks could always be seen. In the following test, the peak numbers of CS-TENG corresponding to different bending angles were tested, which are shown in Figure 4B. When the PTFE film rubs with two electrodes, the bending angle of the actuator is about 10°. At the same time, there will be two peaks in the output signal. From the following graphs, it can be found that when the PTFE film rubbed with one more electrode, the bending angle of the actuator increased by 5°, and there would be one more peak in the output signal. The bending angle of the actuator is linear with the number of electrodes rubbed by the PTFE film. Therefore, this CS-TENG sensor can detect the bending angle with the minimum resolution of 5°. In addition, the resolution can still be further improved by decreasing the distance of each comb-shaped electrode. The comparison of the proposed CS-TENG against other solutions has been listed in Table S2. Compared with the gear-structural bending sensor developed by Sun et al. [26], this CS-TENG is much easier to be fabricated and still has a high angular resolution.

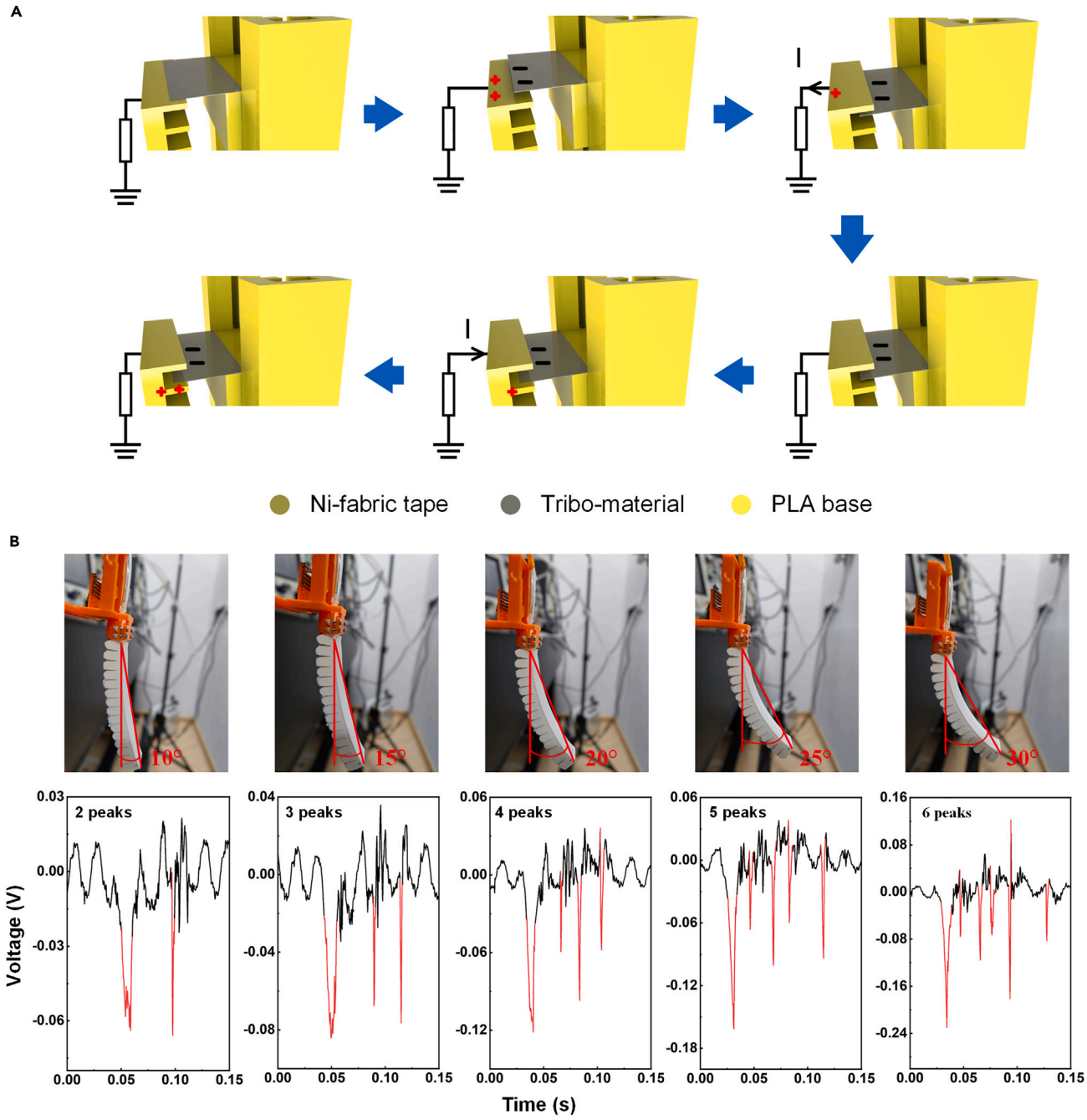

Figure 4. Working mechanism and characterization of CS-TENG

(A) The mechanism and basic structure of CS-TENG.

(B) The peak numbers of CS-TENG corresponding to different bending angles.

Soft robot

There are various driving methods for soft robots; we choose the pneumatic way since it is the simplest one. There are two common materials to make soft robots, silicone rubber and TPUs. We choose TPU, a kind of flexible 3D printing material, to fabricate the soft robot, which is composed of three soft actuators. The cutaway view of the soft actuator with a hollow-bellows structure is shown in Figure S5. The upper surface of the actuator is designed as a corrugated structure with lower stiffness and higher stretchability.

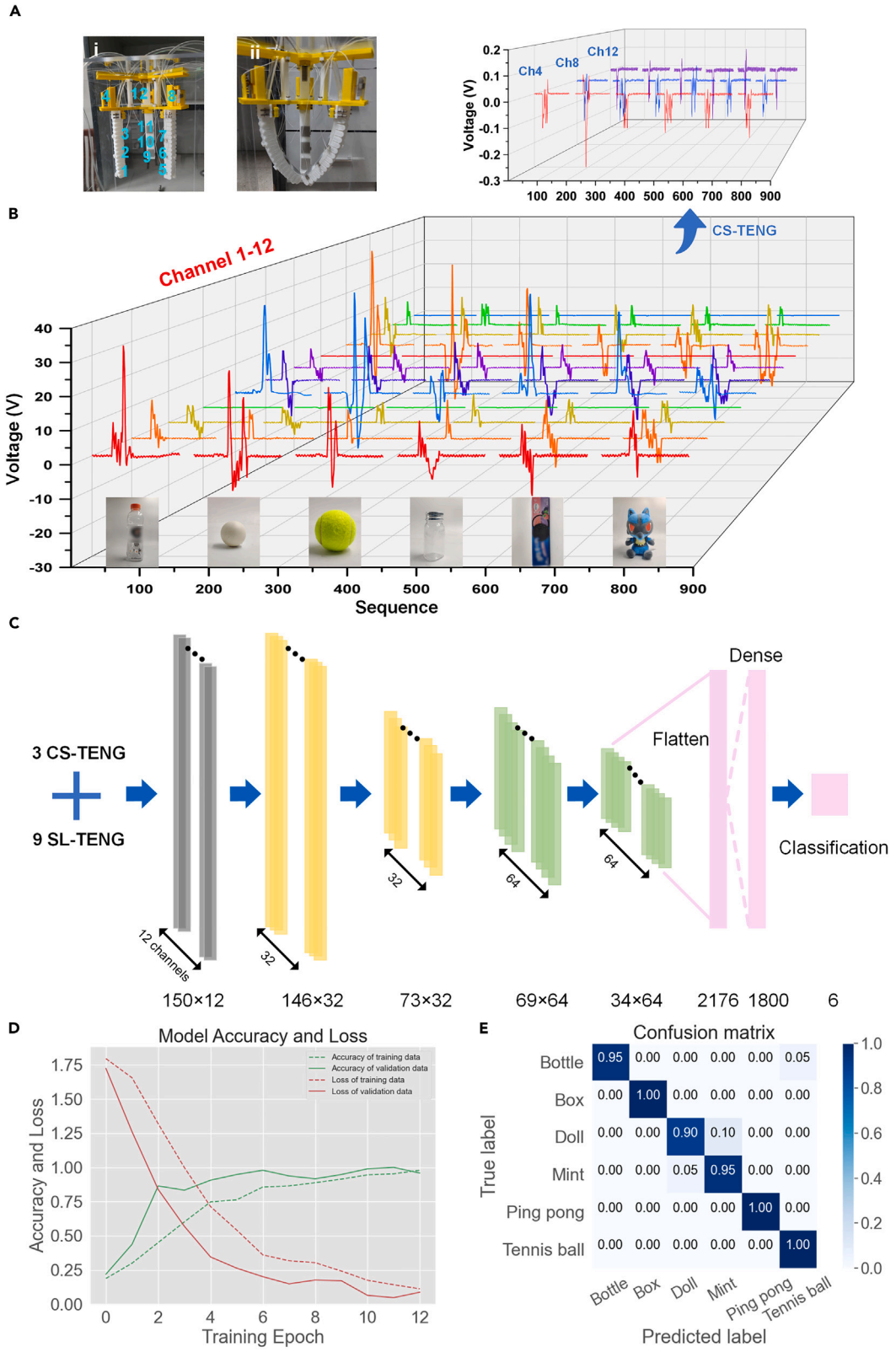
A
i
ii
Ch4
Ch8
Ch12
Voltage (V)
B
Channel 1-12
CS-TENG
Voltage (V)
Sequence
C
3 CS-TENG
9 SL-TENG
12 channels
32
32
64
64
Flatten
Dense
Classification
150×12
146×32
73×32
69×64
34×64
2176
1800
6
D
Model Accuracy and Loss
Accuracy of training data
Accuracy of validation data
Loss of training data
Loss of validation data
Accuracy and Loss
Training Epoch
E
Confusion matrix
Bottle
Box
Doll
Mint
Ping pong
Tennis ball
True label
Predicted label

Figure 5. Data collecting and processing of the sensing system

(A) The image of soft robot. (i) The un-inflated status of soft robot. (ii) The inflated status of soft robot.

(B) 3D plots of the robotic sensor outputs responding to different objects (bottle, ping pong, tennis ball, mint, box, and doll).

(C) The structure of the 1D-CNN.

(D) The learning curve.

(E) The confusion matrix.

Meanwhile, the lower surface is made of the same material without the corrugated structure, which is relatively harder to deform. Therefore, when the soft actuator is inflated, there will be a larger deformation on the upper surface, making the soft actuator bend down. Besides, the increasing air pressure enlarges the bulge of the soft material and results in the larger curvature and output force of the soft actuator. When a certain amount of air pressure is applied, the three actuators of the soft manipulator will bend simultaneously, thereby exerting a three-sided balanced contact force on the object and realizing the function of grasping. The whole soft actuator is directly printed by the 3D printer; the model and the printing parameters are shown in Figure S5. To drive the soft actuator, a set of the pneumatic system is necessary, which is shown in Figure S6. The base of the manipulator was designed and printed out. After assembling all the components referred to earlier, the manipulator was fixed in an acrylic box, which is shown in Figure 5A.

Data processing via one-dimensional convolutional neural network (1D-CNN)

After connecting the soft robot with the pneumatic system and data transmitting system, the whole sensing system is developed, which is shown in Figure S7. Since there are 9 SL-TENGs and 3 CS-TENGs on the manipulator, there will be 12 channels of signal, which contains much hidden information, like position, contact area, bending degree, etc. Moreover, machine learning has been proved to be a good tool to extract features from such data sequences and address classification tasks. Herein, we apply a 1D-CNN to process the data. The dataset contains six objects—bottle, ping pong, tennis ball, mint, box, and doll. To guarantee the amount of training data, each object was grasped for 100 times. The data length for each object is 150, so there were 12 channels×150 = 1,800 features in total for each sample. The 3D plots of the sensor output corresponding to the six objects are shown in Figure 5B. The 100 samples of each object are randomly divided into the training, validation, and testing set at a ratio of 6:2:2. The structure of the developed 1D-CNN is shown in Figure 5C, and the related parameters are shown in Table S3.

After sending the data into the model for training, the learning curve for both the training and validation dataset is shown in Figure 5D. It can be found that the training was stopped at the twelfth epoch, where the accuracy of training data reached 90.89%. Then the trained model was checked against test data, which had not been seen by the model yet. The accuracy of the test data was 98.96%. The confusion matrix is shown in Figure 5E, which means the model generalized well for these objects and shows the power of 1D-CNN. The model was then used to do the real-time object recognition, and the result is shown in Video S1 and Table S4. We tested this sensing system 100 times, and the results of the one-hundredth test were almost the same as those of the first one, which verifies the stability of this sensing system. The recognition results of box, doll, mint, and ping pong are perfect. However, the accuracy of the bottle is lower than other objects. There are two reasons for this phenomenon. The first one is that the TENG signal is vulnerable to environmental interference. There may be some subtle differences between the signal generated during the real-time testing and the original one. The second reason is that the contact area between the bottle and the actuators was very small since the bottle was vertical when it was gripped, which will lead to less effective signals generated by SL-TENG than other objects. Nevertheless, this result still shows the fact that TENG can detect the contact area, pressure, etc. and generate different waveforms. And 1D-CNN can derive the features from the waveform and be used for real-time object recognition. We also tested another four objects to validate the accuracy of this model. The 3D plots of the robotic sensor outputs responding to these four objects are shown in Figure S8. At this time, the accuracy of object recognition is 98%.

Conclusions

In summary, a bionic sensing system, composed of TENG-based intelligent soft robotic fingers was developed. Two new structures of SL-TENG were proposed and tested. Compared with pyramid microstructure in small size, the sensitivity of SL-TENG with the hemispherical microstructure has increased by 7%. And the output of SL-TENG can remain stable after 20,000 times press. Several structures of CS-TENG as the

curvature sensor are proposed, and the model with integrated electrode has the best performance, which has stable signal to represent the curvature by the number of peaks. Three soft actuators were printed out with TPU and assembled with other components to serve as a sensing system, which is demonstrated to be controlled precisely by air pressure. The data generated by the sensors are sent to the computer and saved as a dataset. A 1D-CNN model is constructed and trained (98.96% accuracy). Finally, real-time object recognition is done, and the performance of this sensing system is good, which shows the potential for digital twin applications.

Limitation of the study

Although the recognition results of box, doll, mint, and ping pong are perfect, the accuracy of the bottle is lower than that of other objects because of small contact area. In future work, a better algorithm is necessary to be developed to achieve the recognition of objects with small contact area.

STAR★METHODS

Detailed methods are provided in the online version of this paper and include the following:

- KEY RESOURCES TABLE
- RESOURCE AVAILABILITY
  - Lead contact
  - Materials availability
  - Data and code availability
- EXPERIMENTAL MODEL AND SUBJECT DETAILS
- METHOD DETAILS
  - Fabrication of SL-TENG
  - Fabrication of CS-TENG
  - Fabrication of soft gripper
  - Test and measurement
- QUANTIFICATION AND STATISTICAL ANALYSIS
- ADDITIONAL RESOURCES

SUPPLEMENTAL INFORMATION

Supplemental information can be found online at https://doi.org/10.1016/j.isci.2023.107249.

ACKNOWLEDGMENTS

This work is financially supported by the National Natural Science Foundation of China (No. 62074029, No. 61804023, No. 61971108), the National Key Research and Development Program of China (No. 2022YFB 3206100), the Key Research and Development Program of Sichuan Province (No. 2022JDTD0020, No. 2020ZHCG0038), the Sichuan Science and Technology Program (No. 2019YJ0198, No. 2020YJ0015), and the Fundamental Research Funds for the Central Universities (No. ZYGX2019Z002).

AUTHOR CONTRIBUTIONS

T.W. conceived the research, designed and carried out the experiments, and prepared the figures and paper. H.D., Z.S., and X.R. ZHANG provided support for the experiments, tests, and analysis. C.L. and X.S. ZHANG conceived the research, supervised the experiments and analysis, and prepared the paper.

DECLARATION OF INTERESTS

The authors declare no competing interests.

Received: February 23, 2023
Revised: May 15, 2023
Accepted: June 26, 2023
Published: June 27, 2023

REFERENCES

1. Gao, S., He, T., Zhang, Z., Ao, H., Jiang, H., and Lee, C. (2021). A Motion Capturing and Energy Harvesting Hybridized Lower-Limb System for Rehabilitation and Sports Applications. Adv. Sci. *8*, 2101834. https://doi.org/10.1002/advs.202101834.

2. Yang, Y., Shi, Q., Zhang, Z., Shan, X., Salam, B., and Lee, C. (2023). Robust triboelectric information-mat enhanced by multi-modality deep learning for smart home. InfoMat *5*, e12360. https://doi.org/10.1002/inf2.12360.

3. Wang, Y., Hu, Z., Wang, J., Liu, X., Shi, Q., Wang, Y., Qiao, L., Li, Y., Yang, H., Liu, J., et al. (2022). Deep Learning-Assisted Triboelectric Smart Mats for Personnel Comprehensive Monitoring toward Maritime Safety. ACS Appl. Mater. Interfaces *14*, 24832–24839. https://doi.org/10.1021/acsami.2c05734.

4. Le, X., Shi, Q., Sun, Z., Xie, J., and Lee, C. (2022). Noncontact Human-Machine Interface Using Complementary Information Fusion Based on MEMS and Triboelectric Sensors. Adv. Sci. *9*, 2201056. https://doi.org/10.1002/advs.202201056.

5. Pang, Y., Zhu, X., Lee, C., and Liu, S. (2022). Triboelectric nanogenerator as next-generation self-powered sensor for cooperative vehicle-infrastructure system. Nano Energy *97*, 107219. https://doi.org/10.1016/j.nanoen.2022.107219.

6. Zhang, Z., Wen, F., Sun, Z., Guo, X., He, T., and Lee, C. (2022). Artificial Intelligence-Enabled Sensing Technologies in the 5G/Internet of Things Era: From Virtual Reality/Augmented Reality to the Digital Twin. Advanced Intelligent Systems *4*, 2100228. https://doi.org/10.1002/aisy.202100228.

7. Guo, X., He, T., Zhang, Z., Luo, A., Wang, F., Ng, E.J., Zhu, Y., Liu, H., and Lee, C. (2021). Artificial Intelligence-Enabled Caregiving Walking Stick Powered by Ultra-Low-Frequency Human Motion. ACS Nano *15*, 19054–19069. https://doi.org/10.1021/acsnano.1c04464.

8. Zhang, Z., Shi, Q., He, T., Guo, X., Dong, B., Lee, J., and Lee, C. (2021). Artificial intelligence of toilet (AI-Toilet) for an integrated health monitoring system (IHMS) using smart triboelectric pressure sensors and image sensor. Nano Energy *90*, 106517. https://doi.org/10.1016/j.nanoen.2021.106517.

9. Shi, Q., Zhang, Z., Yang, Y., Shan, X., Salam, B., and Lee, C. (2021). Artificial Intelligence of Things (AIoT) Enabled Floor Monitoring System for Smart Home Applications. ACS Nano *15*, 18312–18326. https://doi.org/10.1021/acsnano.1c07579.

10. Wang, H., Totaro, M., and Beccai, L. (2018). Toward Perceptive Soft Robots: Progress and Challenges. Adv. Sci. *5*, 1800541. https://doi.org/10.1002/advs.201800541.

11. Sun, W., Li, B., Zhang, F., Fang, C., Lu, Y., Gao, X., Cao, C., Chen, G., Zhang, C., and Wang, Z.L. (2021). TENG-Bot: Triboelectric nanogenerator powered soft robot made of uni-directional dielectric elastomer. Nano Energy *85*, 106012. https://doi.org/10.1016/j.nanoen.2021.106012.

12. Liu, Y., Chen, B., Li, W., Zu, L., Tang, W., and Wang, Z.L. (2021). Bioinspired Triboelectric Soft Robot Driven by Mechanical Energy. Adv. Funct. Mater. *31*, 2104770. https://doi.org/10.1002/adfm.202104770.

13. Chen, J., Han, K., Luo, J., Xu, L., Tang, W., and Wang, Z.L. (2020). Soft robots with self-powered configurational sensing. Nano Energy *77*, 105171. https://doi.org/10.1016/j.nanoen.2020.105171.

14. Chen, Y., Pu, X., Liu, M., Kuang, S., Zhang, P., Hua, Q., Cong, Z., Guo, W., Hu, W., and Wang, Z.L. (2019). Shape-Adaptive, Self-Healable Triboelectric Nanogenerator with Enhanced Performances by Soft Solid-Solid Contact Electrification. ACS Nano *13*, 8936–8945. https://doi.org/10.1021/acsnano.9b02690.

15. Chen, J., Chen, B., Han, K., Tang, W., and Wang, Z.L. (2019). A Triboelectric Nanogenerator as a Self-Powered Sensor for a Soft-Rigid Hybrid Actuator. Adv. Mater. Technol. *4*, 1900337. https://doi.org/10.1002/admt.201900337.

16. Rus, D., and Tolley, M.T. (2015). Design, fabrication and control of soft robots. Nature *521*, 467–475. https://doi.org/10.1038/nature14543.

17. Boyraz, P., Runge, G., and Raatz, A. (2018). An Overview of Novel Actuators for Soft Robotics. Actuators *7*, 48. https://doi.org/10.3390/act7030048.

18. Zhang, Q., Zuo, J., Yu, T., and Wang, Y. (2017). Visual recognition system of cherry picking robot based on Lab color model. In IOP Conference Series: Earth and Environmental Science (IOP publishing).

19. Chen, Z., Shen, Y., Xi, N., and Tan, X. (2007). Integrated sensing for ionic polymer-metal composite actuators using PVDF thin films. Smart Mater. Struct. *16*, S262–S271. https://doi.org/10.1088/0964-1726/16/2/s10.

20. Liu, L., Shi, Q., Guo, X., Zhang, Z., and Lee, C. (2023). A facile frequency tuning strategy to realize vibration-based hybridized piezoelectric-triboelectric nanogenerators. Ecomat *5*, e12279. https://doi.org/10.1002/eom2.12279.

21. Tang, G., Wang, Z., Hu, X., Wu, S., Xu, B., Li, Z., Yan, X., Xu, F., Yuan, D., Li, P., et al. (2022). A Non-Resonant Piezoelectric-Electromagnetic-Triboelectric Hybrid Energy Harvester for Low-Frequency Human Motions. Nanomaterials *12*, 1168. https://doi.org/10.3390/nano12071168.

22. Le, X., Shi, Q., Vachon, P., Ng, E.J., and Lee, C. (2022). Piezoelectric MEMS-evolution from sensing technology to diversified applications in the 5G/Internet of Things (IoT) era. J. Micromech. Microeng. *32*, 014005. https://doi.org/10.1088/1361-6439/ac3ab9.

23. Liu, H., Quan, C., Tay, C.J., Kobayashi, T., and Lee, C. (2011). A MEMS-based piezoelectric cantilever patterned with PZT thin film array for harvesting energy from low frequency vibrations. Phys. Proc. *19*, 129–133.

24. Zhou, L., Zhu, L., Yang, T., Hou, X., Du, Z., Cao, S., Wang, H., Chou, K.-C., and Wang, Z.L. (2021). Ultra-Stable and Durable Piezoelectric Nanogenerator with All-Weather Service Capability Based on N Doped 4H-SiC Nanohole Arrays. Nano-Micro Lett. *14*, 30. https://doi.org/10.1007/s40820-021-00779-0.

25. Song, S., Li, Z., Meng, M.Q.H., Yu, H., and Ren, H. (2015). Real-Time Shape Estimation for Wire-Driven Flexible Robots With Multiple Bending Sections Based on Quadratic Bezier Curves. IEEE Sens. J. *15*, 6326–6334. https://doi.org/10.1109/jsen.2015.2456181.

26. Peng, L., Zhang, Y., Wang, J., Wang, Q., Zheng, G., Li, Y., Chen, Z., Chen, Y., Jiang, L., and Wong, C.-P. (2022). Slug-inspired Magnetic Soft Millirobot Fully Integrated with Triboelectric Nanogenerator for On-board Sensing and Self-powered Charging. Nano Energy *99*, 107367. https://doi.org/10.1016/j.nanoen.2022.107367.

27. Hu, C., Yang, Y., and Wang, Z.L. (2022). Quantitative comparison between the effective energy utilization efficiency of triboelectric nanogenerator and electromagnetic generator post power management. Nano Energy *103*, 107760. https://doi.org/10.1016/j.nanoen.2022.107760.

28. Tairych, A., and Anderson, I.A. (2019). Capacitive Stretch Sensing for Robotic Skins. Soft Robot. *6*, 389–398. https://doi.org/10.1089/soro.2018.0055.

29. Gao, S., Zeng, X., Zhang, G., Zhang, J., Chen, Y., Feng, S., Lan, W., Zhou, J., and Wang, Z.L. (2022). Triboelectric-electromagnetic hybridized module for energy harvesting of power transmission lines galloping and self-powered galloping state monitoring. Nano Energy *101*, 107530. https://doi.org/10.1016/j.nanoen.2022.107530.

30. Tian, W., Wakimoto, S., Kanda, T., and Yamaguchi, D. (2022). Displacement Sensing of an Active String Actuator Using a Step-Index Multimode Optical Fiber Sensor. Sensors *22*, 3232. https://doi.org/10.3390/s22093232.

31. Wu, X.S., Zhang, Z.H., Zhao, F., Wang, W.J., Li, Y.F., Bi, L., Qian, Z.Z., Lu, S.S., Feng, F., Hu, C.Y., et al. (2016). A novel energy conversion method based on hydrogel material for self-powered sensor system applications. J. Adolesc. *52*, 103–111. https://doi.org/10.1016/j.apenergy.2016.04.028.

32. Deng, H.-T., Zhang, X.-R., Wang, Z.-Y., Wen, D.-L., Ba, Y.-Y., Kim, B., Han, M.-D., Zhang, H.-X., and Zhang, X.-S. (2021). Super-stretchable multi-sensing triboelectric nanogenerator based on liquid conductive composite. Nano Energy *83*, 105823. https://doi.org/10.1016/j.nanoen.2021.105823.

33. Huang, P., Wen, D.-L., Qiu, Y., Yang, M.-H., Tu, C., Zhong, H.-S., and Zhang, X.-S. (2021).

Textile-Based Triboelectric Nanogenerators for Wearable Self-Powered Microsystems. Micromachines *12*, 158. https://doi.org/10.3390/mi12020158.

34. Ba, Y.-Y., Bao, J.-F., Deng, H.-T., Wang, Z.-Y., Li, X.-W., Gong, T., Huang, W., and Zhang, X.-S. (2020). Single-Layer Triboelectric Nanogenerators Based on Ion-Doped Natural Nanofibrils. ACS Appl. Mater. Interfaces *12*, 42859–42867. https://doi.org/10.1021/acsami.0c11932.

35. Liu, D., Bao, J.-F., Chen, Y.-L., Li, G.-K., and Zhang, X.-S. (2020). Unidirectional-current triboelectric nanogenerator based on periodical lateral-cantilevers. Nano Energy *74*, 104770. https://doi.org/10.1016/j.nanoen.2020.104770.

36. Wen, D.-L., Liu, X., Deng, H.-T., Sun, D.-H., Qian, H.-Y., Brugger, J., and Zhang, X.-S. (2019). Printed silk-fibroin-based triboelectric nanogenerators for multi-functional wearable sensing. Nano Energy *66*, 104123. https://doi.org/10.1016/j.nanoen.2019.104123.

37. Deng, H.-T., Wang, Z.-Y., Wang, Y.-L., Wen, D.-L., and Zhang, X.-S. (2022). Integrated hybrid sensing and microenergy for compact active microsystems. Microsyst. Nanoeng. *8*, 61. https://doi.org/10.1038/s41378-022-00393-z.

38. Wang, H.L., Guo, Z.H., Pu, X., and Wang, Z.L. (2022). Ultralight Iontronic Triboelectric Mechanoreceptor with High Specific Outputs for Epidermal Electronics. Nano-Micro Lett. *14*, 86. https://doi.org/10.1007/s40820-022-00834-4.

39. Ba, Y.-Y., Bao, J.-F., Wang, Z.-Y., Deng, H.-T., Wen, D.-L., Zhang, X.-R., Tu, C., and Zhang, X.-S. (2021). Self-powered trajectory-tracking microsystem based on electrode-miniaturized triboelectric nanogenerator. Nano Energy *82*, 105730. https://doi.org/10.1016/j.nanoen.2020.105730.

40. Liang, C., and Han, M. (2019). Applications in Biomedical Systems. In Flexible and Stretchable Triboelectric Nanogenerator Devices, pp. 339–358. https://doi.org/10.1002/9783527820153.ch17.

41. Guo, Y., Zhang, X.-S., Wang, Y., Gong, W., Zhang, Q., Wang, H., and Brugger, J. (2018). All-fiber hybrid piezoelectric-enhanced triboelectric nanogenerator for wearable gesture monitoring. Nano Energy *48*, 152–160. https://doi.org/10.1016/j.nanoen.2018.03.033.

42. Zhang, X.-S., Han, M., Kim, B., Bao, J.-F., Brugger, J., and Zhang, H. (2018). All-in-one self-powered flexible microsystems based on triboelectric nanogenerators. Nano Energy *47*, 410–426. https://doi.org/10.1016/j.nanoen.2018.02.046.

43. Zhang, X.-S., Brugger, J., and Kim, B. (2016). A silk-fibroin-based transparent triboelectric generator suitable for autonomous sensor network. Nano Energy *20*, 37–47. https://doi.org/10.1016/j.nanoen.2015.11.036.

44. Zhang, Y., Fan, K., Zhu, J., Wu, S., Zhang, S., Cheng, T., and Wang, Z.L. (2022). Multi-purpose triboelectric-electromagnetic hybrid nanogenerator with a mechanical motion-controlled switch for harvesting low-frequency energy. Nano Energy *104*, 107867. https://doi.org/10.1016/j.nanoen.2022.107867.

45. Hu, S., Han, J., Shi, Z., Chen, K., Xu, N., Wang, Y., Zheng, R., Tao, Y., Sun, Q., Wang, Z.L., and Yang, G. (2022). Biodegradable, Super-Strong, and Conductive Cellulose Macrofibers for Fabric-Based Triboelectric Nanogenerator. Nano-Micro Lett. *14*, 115. https://doi.org/10.1007/s40820-022-00858-w.

46. Ning, C., Wei, C., Sheng, F., Cheng, R., Li, Y., Zheng, G., Dong, K., and Wang, Z.L. (2023). Scalable one-step wet-spinning of triboelectric fibers for large-area power and sensing textiles. Nano Res. *16*, 7518–7526. https://doi.org/10.1007/s12274-022-5273-7.

47. Zhang, R., Hummelgård, M., Örtegren, J., Olsen, M., Andersson, H., Yang, Y., Olin, H., and Wang, Z.L. (2022). Utilising the triboelectricity of the human body for human-computer interactions. Nano Energy *100*, 107503. https://doi.org/10.1016/j.nanoen.2022.107503.

48. Pu, X., Zhang, C., and Wang, Z.L. (2023). Triboelectric nanogenerators as wearable power sources and self-powered sensors. Natl. Sci. Rev. *10*, nwac170. https://doi.org/10.1093/nsr/nwac170.

49. Zhu, M., Xie, M., Lu, X., Okada, S., and Kawamura, S. (2020). A soft robotic finger with self-powered triboelectric curvature sensor based on multi-material 3D printing. Nano Energy *73*, 104772. https://doi.org/10.1016/j.nanoen.2020.104772.

50. Pu, X., Guo, H., Tang, Q., Chen, J., Feng, L., Liu, G., Wang, X., Xi, Y., Hu, C., and Wang, Z.L. (2018). Rotation sensing and gesture control of a robot joint via triboelectric quantization sensor. Nano Energy *54*, 453–460. https://doi.org/10.1016/j.nanoen.2018.10.044.

51. Qu, X., Liu, Z., Tan, P., Wang, C., Liu, Y., Feng, H., Luo, D., Li, Z., and Wang, Z.L. (2022). Artificial tactile perception smart finger for material identification based on triboelectric sensing. Sci. Adv. *8*, eabq2521. https://doi.org/10.1126/sciadv.abq2521.

52. Jin, G., Sun, Y., Geng, J., Yuan, X., Chen, T., Liu, H., Wang, F., and Sun, L. (2021). Bioinspired soft caterpillar robot with ultra-stretchable bionic sensors based on functional liquid metal. Nano Energy *84*, 105896. https://doi.org/10.1016/j.nanoen.2021.105896.

53. Chen, S., Pang, Y., Yuan, H., Tan, X., and Cao, C. (2020). Smart Soft Actuators and Grippers Enabled by Self-Powered Tribo-Skins. Adv. Mater. Technol. *5*, 1901075. https://doi.org/10.1002/admt.201901075.

54. Jin, T., Sun, Z., Li, L., Zhang, Q., Zhu, M., Zhang, Z., Yuan, G., Chen, T., Tian, Y., Hou, X., and Lee, C. (2020). Triboelectric nanogenerator sensors for soft robotics aiming at digital twin applications. Nat. Commun. *11*, 5381. https://doi.org/10.1038/s41467-020-19059-3.

55. Sun, Z., Zhu, M., Zhang, Z., Chen, Z., Shi, Q., Shan, X., Yeow, R.C.H., and Lee, C. (2021). Artificial Intelligence of Things (AIoT) Enabled Virtual Shop Applications Using Self-Powered Sensor Enhanced Soft Robotic Manipulator. Adv. Sci. *8*, 2100230. https://doi.org/10.1002/advs.202100230.

56. Lai, Y.-C., Deng, J., Liu, R., Hsiao, Y.-C., Zhang, S.L., Peng, W., Wu, H.-M., Wang, X., and Wang, Z.L. (2018). Actively Perceiving and Responsive Soft Robots Enabled by Self-Powered, Highly Extensible, and Highly Sensitive Triboelectric Proximity- and Pressure-Sensing Skins. Adv. Mater. *30*, 1801114. https://doi.org/10.1002/adma.201801114.

57. Lee, S., and Park, J.-W. (2022). Fingerprint-inspired triboelectric nanogenerator with a geometrically asymmetric electrode design for a self-powered dynamic pressure sensor. Nano Energy *101*, 107546. https://doi.org/10.1016/j.nanoen.2022.107546.

STAR★METHODS

KEY RESOURCES TABLE

REAGENT or RESOURCE	SOURCE	IDENTIFIER
Chemicals, peptides, and recombinant proteins		
PI	Runhai office flagship store (Taobao, China)	N/A
PTFE	Ouwen flagship store (Taobao, China)	N/A
Eco-flex 00–30 silicone	Dongzhixuan store (Taobao, China)	N/A
Software and algorithms		
PyCharm	IntelliJ Software s.r.o.	N/A
Arduino IDE	Arduino LCC	N/A
SOLIDWORKS	Dassault Systèmes SOLIDWORKS Corp	N/A
ideaMaker	Raise 3D Technologies, Inc	N/A

RESOURCE AVAILABILITY

Lead contact

Further information and requests for resources and reagents should be directed to and will be fulfilled by the lead contact, Xiaosheng Zhang (zhangxs@uestc.edu.cn).

Materials availability

This study did not generate new materials. Materials used in the study are commercially available.

Data and code availability

All data reported in this paper will be shared by the lead contact upon reasonable request.

No new code was generated during the course of this study.

Any additional information required to reanalyze the data reported in this paper is available from the lead contact upon reasonable request.

EXPERIMENTAL MODEL AND SUBJECT DETAILS

This study does not use experimental methods typical in the life sciences.

METHOD DETAILS

Fabrication of SL-TENG

All experimental materials such as silicone and Ni-fabric tape were purchased from a local market (as shown in key resources table) and used without further treatment. The bottom side length of each micro-structure is 1.5mm and the height is 2.5 mm. The interval distance of them is 1 mm. To make this structure of tribo-skin, a mold was needed first (polylactic acid (PLA) mold for Pyramid microstructure in a big size and aluminum mold for Pyramid and hemispherical microstructure in a small size). In the next step, Eco-flex 00–30 silicone solutions were used (part A and part B were mixed at a ratio of 1:1 first) and poured into the mold. After being evacuated to eliminate bubbles by a vacuum pump, the mold was put in the oven (40°C and 60 min for PLA mold and 70°C and 15 min for aluminum mold). Finally, the molded silicone rubber was peeled off from the mold and stuck with the Ni-fabric tape. The TENG's length, width and thickness are 25 mm, 22 mm and 1.5 mm respectively.

Fabrication of CS-TENG

All experimental materials such as PTFE, PLA, PI and Ni-fabric tape were purchased from a local market (as shown in key resources table) and used without further treatment. Teflon tube is connected with the end of the soft manipulator. PTFE film is fixed on the PLA base, which will rub with the combed electrode during

the process of bending. A 75 μm PI film is attached to the top of the base. At the bottom of the base, there is a circular hole to fix the Teflon tube. On the top of the base, there is a hook to be connected with a spring. The other end of the spring is connected with the top component. There is also a slide rail to fix the moving direction of the base. Finally, Ni-fabric tape is stuck on the protruding part of the printed model to serve as the electrode.

Fabrication of soft gripper

The soft gripper with a bellows-structured actuator was designed by software (Solidworks 2021, as shown in key resources table). To ensure elastic property and output force, TPU filament with a hardness of shore 85 A was used to fabricate the soft actuator. The filament was extruded by Titan Extruder and the printing temperature is 240°C with a corresponding low printing speed of 20 mm/s. The layer thickness was changed to 0.1 mm to guarantee the printing precision.

Test and measurement

The surface morphologies of the silicone rubber with the hemispherical structure were characterized using scanning electron microscopy (SEM, JSM-6490LV, JEOL Ltd.). A vibration platform consisting of a signal generating system (33250A, Agilent), an amplifier and a shaker was used to provide a stable and controllable force with designable frequency to the device. The triboelectric voltage outputs were measured using a digital oscilloscope (DS2302A, RIOGL) with a 100 MΩ probe, and the triboelectric current outputs were measured by a low-noise current preamplifier (SR570, Stanford Research Systems) and a digital oscilloscope (DS2302A, RIOGL) with a 100 MΩ probe.

QUANTIFICATION AND STATISTICAL ANALYSIS

The data was measured by a digital oscilloscope (DS2302A, RIOGL) with a 100 MΩ probe, and the triboelectric current outputs were measured by a low-noise current preamplifier (SR570, Stanford Research Systems) and a digital oscilloscope (DS2302A, RIOGL) with a 100 MΩ probe. Figures were produced by Origin from the raw data.

ADDITIONAL RESOURCES

This study has not generated or contributed to a new website/forum.